THE JOURNAL OF PHYSICAL CHEMISTRY C

ARTICLE

pubs.acs.org/JPCC

Diverging Geometric and Magnetic Size Distributions of Iron Oxide Nanocrystals

Bob Luigjes,[†] Suzanne M. C. Woudenberg,[†] Rick de Groot,[†] Johannes D. Meeldijk,[‡] Hirsa M. Torres Galvis,[¶] Krijn P. de Jong,[¶] Albert P. Philipse,[†] and Ben H. Erné*[,†]

[†]Van 't Hoff Laboratory for Physical and Colloid Chemistry, [‡]Electron Microscopy, and [¶]Inorganic Chemistry and Catalysis Group, Debye Institute for Nanomaterials Science, Utrecht University, Padualaan 8, 3584 CH Utrecht, The Netherlands

Supporting Information

ABSTRACT: An important reason to prepare magnetic nanoparticles of uniform size and shape is to ensure uniform magnetic properties. However, here, we demonstrate that magnetic iron oxide crystals of 20 nm or less with a low polydispersity of the geometric size can nevertheless have a strikingly broad distribution of the magnetic dipole moment. A comparative study was performed on nanoparticles with near-perfect crystallinity, twinning defects, or a high density of dislocations. Size, shape, and crystal defects were characterized with electron microscopy and X-ray diffraction, and magnetic dipole moments were determined from magnetization curves of dilute colloidal dispersions. The largest divergence was found for spherical particles with 3.5% geometric size polydispersity and 35% magnetic size polydispersity due to crystal lattice defects that disrupt single-domain magnetic spin coupling. This is in stark contrast with the usual implicit assumption that uniform size and shape guarantee well-defined magnetic properties of the individual particles.

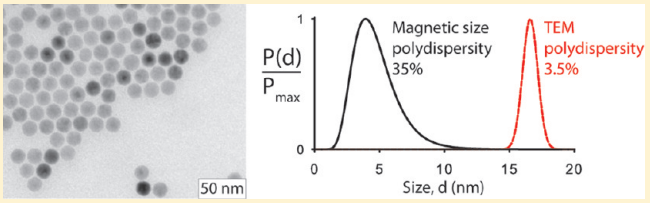

1. INTRODUCTION

Magnetic nanoparticles have generated much interest, thanks to their suitability for many applications in the fields of magnetic data storage, catalysis, and biomedicine.[1−13] For applications that require uniform magnetic properties of the individual particles, a uniform size is critical because the magnetic properties of nanoparticles are strongly size-dependent.[14] Fortunately, it is possible to prepare nanoparticles with a low polydispersity, down to a few percent. However, we will demonstrate that due to crystal defects, particles of 20 nm or less with a low polydispersity of the geometric size can, nevertheless, have a high polydispersity of the magnetic properties.

An example of an application in which uniform magnetic properties are critical is the use of magnetic nanoparticles to obtain locally targetted therapeutic hyperthermia.[3,9,15−17] The particles are introduced into a patient, in the vicinity of biological cells to be destroyed, and they are selectively heated using an alternating magnetic field. In theory, the most effective heating is produced when the characteristic frequency for magnetic relaxation is the same for each particle and the alternating field is applied at precisely that frequency. In practice, polydispersity of nanoparticle size diminishes the magnetic heating that can be achieved,[17] and the theoretical limit seems almost impossible to reach because small differences in size can already cause large differences in the magnetization dynamics. For instance, an increase in the radius of magnetite nanoparticles (Fe_3O_4) from 7 to 8 nm theoretically slows down the Néel mobility of the magnetic dipole by a factor of 50,[16] a size sensitivity confirmed by frequency-dependent magnetic susceptibility measurements.[18]

Another application of nanoparticles for which uniform magnetic properties are crucial[19] is as tracer material for magnetic particle imaging,[20] an emerging technique that gives the prospect of performing rapid tomographic imaging using relatively inexpensive single-sided scanners.[21]

Nanoparticles with a low geometric size polydispersity can be prepared by thermal decomposition of organometallic precursors.[1,5,6,10,22−24] Obtaining size uniformity relies on the separation of nucleation and growth processes. A brief nucleation event yields initial particles that subsequently all grow at the same rate under conditions that no new nuclei are formed. We expect magnetic iron oxide crystals of 20 nm or less to have a single magnetic domain,[25,26] in which case particles of the same size should all have the same permanent magnetic dipole moment. Nevertheless, due to crystal defects, the magnetic polydispersity is likely to be greater than expected from the geometric size polydispersity.

The most widely invoked type of defect has only a moderate effect: it consists of a "magnetically dead" surface layer on the order of 1 nm that effectively does not contribute to the magnetic dipole moment of the particle.[14,27−30] In this paper, we focus on internal defects whose effect on the magnetic properties is more detrimental. Magnetic measurements are performed on iron oxide nanoparticles with twinning defects or a high density of

Received: April 11, 2011
Revised: June 16, 2011
Published: June 20, 2011

ACS Publications © 2011 American Chemical Society

dislocations, and a comparison is made with iron oxide particles of the same size but with near-perfect single crystallinity.

In Section 2, the chemical synthesis and characterization methods are described. This includes a discussion of our approach to determine magnetic dipole moment distributions, by analyzing magnetization curves measured on dilute colloidal dispersions (Section 2.3). In Section 3, the experimental results obtained by electron microscopy, magnetization measurements, and X-ray diffraction are presented. Finally, in Section 4, the results are discussed for the different types of particles studied, with a low or a high geometric size polydispersity and a low or a high magnetic polydispersity.

2. EXPERIMENTAL METHODS

2.1. Chemical Synthesis Methods. Magnetic iron oxide nanocrystals were prepared by different methods, resulting in particles that are referred to as "facets", "precipitates", "twins", and "spheres". The main aspects of the chemical syntheses are given below. The synthesis of the "twins" is described in the most detail because it has not been published before.

Our preparation of the "facets", already reported elsewhere,[31] is similar to the method of Sun et al.[32,33] Briefly, initial seeds with a size of 5 nm were grown in 14 seeded growth steps to a final size of 20 nm. Iron acetylacetonate was thermally decomposed in diphenyl ether in the presence of oleic acid, oleyl amine, and 1,2-hexadecanediol. The synthesis was performed under nitrogen on a 20 mL scale, and the reaction mixture was heated to reflux without stopping to degas and then refluxed for 30 min. The "facet" particles were used previously in several studies of dipolar structure formation.[34−39]

The "twins" were prepared according to a variation on the procedure to prepare the "facets", in 27 seeded growth steps. First, seed particles of a few nanometers in size were prepared by mixing 7.06 g (20 mmol) of iron acetylacetonate (Acros, >99%), 20.23 g (100 mmol) of 1,2-dodecanediol (Aldrich, 90%), 16.90 g (60 mmol) of oleic acid (Sigma-Aldrich, 90%), and 16.04 g (60 mmol) of oleyl amine (Fluka, >70%) in 200 mL of phenyl ether (Acros, 99%). This reaction mixture was heated to 200 °C under nitrogen flow to degas the dispersion for 30 min, after which the mixture was heated to reflux temperature (around 260 °C) for another 30 min under nitrogen atmosphere. The resulting seed dispersion was washed by precipitation with 100 mL of ethanol and 30−40 min of centrifugation at 2000 rpm (912*g*). These seed particles were redispersed in hexane (Merck, p.a.) and grown in repeated seeded-growth steps using the same procedure as described above, with only the amounts of surfactants (oleic acid and oleyl amine) reduced to 20 mmol. After 20 growth steps when the particles did not seem to grow any further, the amounts of surfactants were decreased to 10 mmol. After each growth step, 10% of the reaction mixture was taken out for storage.

The "precipitates" were prepared by Bica[40] by aqueous precipitation of iron salts according to a method similar to that of Massart,[41] followed by transfer to the apolar solvent decalin after surface modification with oleic acid. The same particles were previously used in a statistical thermodynamics study that involved determining the size of 10^5 particles, confirming a log-normal shape of the distribution.[42]

The "spheres" were made by single-step thermal decomposition of iron oleate using a method from the Hyeon group.[43,44] The syntheses were performed with 20 mL of solvent, 3 mmol of iron oleate, and ∼0.8 g of oleic acid. To obtain uniform particles, it was important to perform the degassing step described by Kwon et al.[44] To vary the average particle size, solvents with different boiling points were used (octadecene, trioctylamine, eicosene).

2.2. Characterization Methods. For transmission electron microscopy (TEM), Philips Tecnai 12 and 20 electron microscopes operating at 120 or 200 kV, respectively, were used. Size distribution parameters were determined from size analysis of 800 of the "precipitate" particles and 200−300 of each of the other types of particles.

To obtain magnetization curves at room temperature, a Micromag 2900 alternating gradient magnetometer from Princeton Measurements, calibrated with an yttrium iron garnet sphere calibration sample purchased from NIST, was used. Dilute dispersions of the nanoparticles in the apolar solvent decalin were contained in square capillary cups of 4 × 4 × 0.4 mm^3 oriented with the 4 × 4 mm^2 face parallel to the magnetic field, to minimize demagnetization effects. Further experimental details are in ref 45.

To determine saturation magnetizations of the particles in emu per gram, including oleic acid layer, magnetization curves were also measured for weighed amounts of dry particles after three washing steps to remove excess oleic acid. In each step, ethanol was used to destabilize the colloidal dispersion, the system was centrifuged, the supernatant was removed, and the particles were redispersed in cyclohexane. In a final step, the cyclohexane was removed by evaporation.

X-ray diffraction measurements were performed with a Bruker AXS D8 Advance diffractometer equipped with a Co Kα1 source (λ = 0.178 897 nm) in a wide angle range (from 22 to 80° in 2θ). The iron oxide crystallite size was determined using the Scherrer equation:[46] $d = K\lambda/[\beta \cos \theta]$, where d is the size of the crystalline domain; K is the shape factor, which is taken to be 0.9 for unknown particle shapes; λ is the wavelength of the incident radiation; β is the line-broadening at half the maximum intensity (fwhm) of the peak in radians; and θ is the Bragg angle in radians.

2.3. Magnetic Analysis Approach. To determine magnetic polydispersities of nanoparticles, we follow an approach known from the field of ferrofluids: the analysis of magnetization curves of dilute colloidal dispersions of the particles in a liquid.[45,47−49] The main underlying principle is that in the liquid, nanoparticle dipoles respond independently of each other to the magnetic field, as long as the dispersion is sufficiently dilute and the dipole moments are not too large.[45,50,51] In this way, effective dipole moments can be obtained for the individual particles with a single magnetic domain (or the internal magnetic domains of particles with multiple domains), regardless of their shape or anisotropy. Magnetic dipole moment distributions are calculated by fitting the magnetization curves on the basis of a log-normal distribution of the dipole moments.

The Langevin function, L (dimensionless), describes the degree of alignment of a dipole of magnitude m (in Am^2) in an external field H (in A/m):

$$L(m,H) = \coth\left(\frac{\mu_0 mH}{k_B T}\right) - \frac{k_B T}{\mu_0 mH} \qquad (1)$$

where μ_0 is the permittivity of vacuum and $k_B T$ is the thermal energy. A log-normal distribution function $P(m)$ (with units $(Am^2)^{-1}$) of the magnetic dipole moment is assumed, as is often

done for ferrofluids,[45,47−51]

$$P(m) = \frac{1}{\sqrt{2\pi}m\sigma_m} \exp\left(-\frac{\left(\ln\frac{m}{m^*}\right)^2}{2\sigma_m{}^2}\right) \quad (2)$$

where $\ln(m^*)$ and σ_m are the mean and the standard deviation of $\ln(m)$. On this basis, the average magnetic dipole moment is $\langle m\rangle = m^* \exp(\sigma_m{}^2/2)$. The total magnetization, M, of the colloidal dispersion (in A/m) is given by

$$M = \chi_{dia}H + \frac{N}{V}\int_0^\infty mP(m)\, L(m,H)\, \mathrm{d}m \quad (3)$$

where χ_{dia} is the diamagnetic susceptibility (dimensionless), N is the total number of magnetic nanoparticles, and V is the system volume (in m^3). $P(m)\,\mathrm{d}m$ gives the number probability to have a particle of dipole moment between m and $m + \mathrm{d}m$, so that an additional factor of m is required to account for the fact that a particle with a small magnetic dipole moment contributes less than a particle with a large magnetic dipole moment to the total magnetic moment of the sample.[48] The linear diamagnetic term is due to the solvent and the sample holder; whether it is negligible depends on the concentration of iron oxide in the ferrofluid. The measurements were corrected for the diamagnetic contribution, a correction whose reliability was confirmed by obtaining the same magnetic dipole moment distribution at different ferrofluid concentrations.

The magnetic sizes d_m that we report are the diameters of hypothetical spherical particles that would have both the same magnetic dipole moment as our particles and the theoretical bulk magnetization, m_s, of magnetite, 91 emu/g (maghemite is on the order of 80 emu/g).[52]

$$d_m = \sqrt[3]{6m/(\pi m_s)} \quad (4)$$

It is noted that this is an effective size and that our particles are spheres only by crude approximation, but there is insufficient detailed information about the three-dimensional shape of our particles and their magnetic domains to warrant describing them with more than one length scale parameter. Furthermore, in contrast to the work of Chen et al.,[49] who took into account the magnetic effect of a defective surface shell, our objective is not to use magnetization measurements to determine the geometric particle size. Our own magnetic sizes are merely a way to express the magnetic dipole moment of the particles in nanometers after conversion using the theoretical magnetization per unit volume as a constant conversion factor.

One complication of expressing the magnetic dipole moment as an effective size is that magnetization measurements yield volume-averaged dipole moments, whereas geometric size distributions from electron microscopy are number-averaged. From eq 4, a log-normal distribution of the magnetic dipole moment implies a log-normal distribution of the magnetic size. The mean, $\ln(m^*)$, and standard deviation, σ_m, of the dipole moment distribution are related to the mean, $\ln(d_m^*)$, and standard deviation, σ_d, of the magnetic size distribution as follows:

$$d_m^* = \sqrt[3]{6m^*/(\pi m_s)} \quad (5)$$

$$\sigma_d = \frac{1}{3}\sigma_m \quad (6)$$

Using eqs 5 and 6, number density distributions were calculated. These can now directly be compared to the TEM size distributions, which were described by a log-normal function, yielding a mean $\ln(d_{TEM}^*)$ and a standard deviation σ_{TEM}. Nevertheless, it is useful also to know the volume averages for better comparison with the volume-averaged XRD values. Therefore, volume-averaged geometric and magnetization sizes were calculated for each type of particle, as well.

3. RESULTS

3.1. Electron Microscopy. Figure 1 illustrates that the various synthesis methods resulted in magnetic iron oxide nanocrystals of different shapes and sizes. The geometric size distributions obtained from TEM are log-normal number density probability functions, and their dimensionless standard deviations are used as a measure of the polydispersity to express how uniform the particles are. The "facets" are faceted particles with an average TEM size of 20 nm and a relatively low TEM polydispersity. The "precipitates" are highly polydisperse maghemite particles. The "twins" have clearly distinguishable twinning defects, and their TEM size and polydispersity are similar to the "facets". Finally, the "spheres" are roughly spherical particles with a low TEM polydispersity.

"Facet" and "sphere" particles with the same size of 20 nm were also examined more closely using high-resolution TEM to study internal crystal defects[53−55] (see Figure 2). At first sight, the crystalline periodicity of the "spheres" appears to extend across the entire particles, at least for the imaged crystal planes. However, on the scale of a few nanometers, the electron contrast of each particle is inhomogeneous, both in bright field (transmitted electrons) and in dark field (diffracted electrons). Contrast depends on whether the orientations of the crystal planes fulfill electron diffraction conditions. For this reason, differently oriented "facet" particles or crystalline domains inside the "twin" particles have sharply different contrasts (Figure 1a,c). In the 20 nm "spheres", such contrast differences are now observed inside individual particles, which can be explained by crystal defects. The dislocation concentration in the 20 nm "spheres" is high (Figure 2f), whereas for comparison, no dislocation is observed for the imaged "facet" particle (Figure 2h).

3.2. Magnetic Measurements. Magnetization curves were measured for colloidal dispersions of the particles with at least two different low volume fractions to demonstrate that interparticle interactions have a negligible effect on the magnetization curve (see the Supporting Information). For the 20 nm "facet" particles, the volume fraction of the colloidal dispersion had to be lower than 0.5%; otherwise, significantly larger average dipole moments and polydispersities were found.[45] The reason is that at higher concentrations, the magnetization curve is no longer that of single particles but of dipolar chains.[34,35,45,51,56] For all the other particles, the results were concentration-independent below concentrations of a few percent. This agrees with the negligible effect of dipolar interactions found at room temperature and concentrations of a few volume percent or lower in previous systematic work on the concentration-dependent magnetic properties of "precipitate"-like particles[51,56,57] and of particles prepared by the same "heating up" method that we used to prepare the "spheres".[58]

The main results are the magnetic size distributions in Figure 1. For the "facets", the "precipitates", and the 8 nm "spheres", TEM

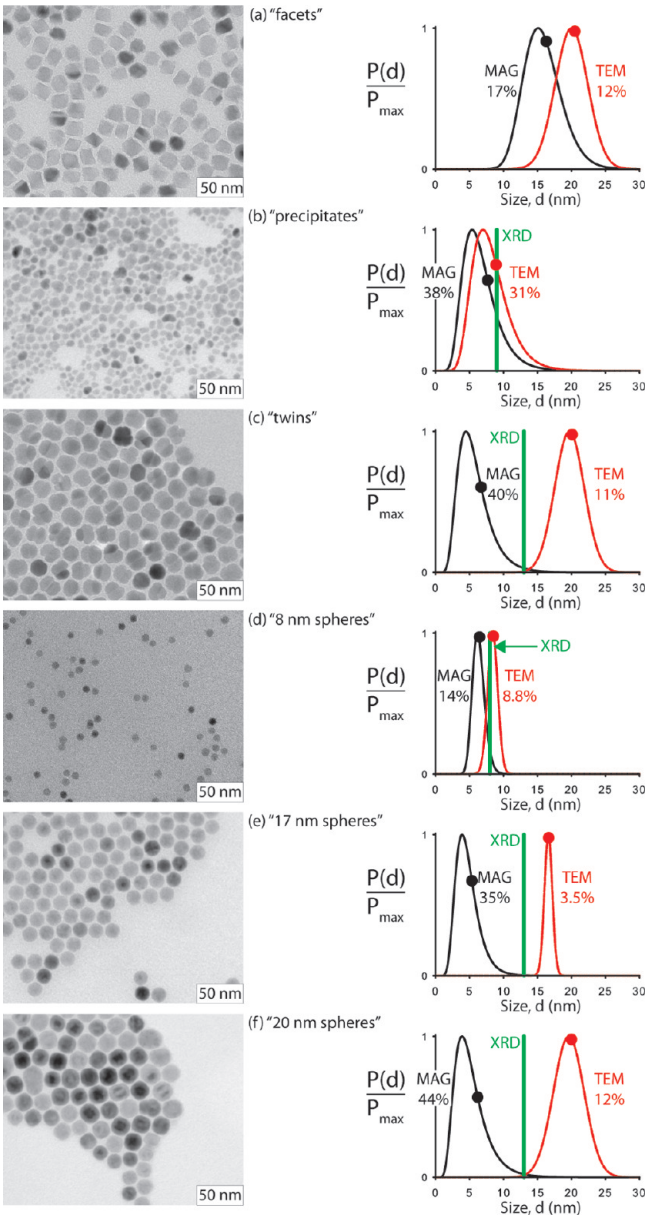

Figure 1. Transmission electron microscopy (TEM) images and size distributions of iron oxide nanoparticles synthesized by different methods: (a) thermal decomposition of iron acetylacetonate, (b) aqueous precipitation, (c) a variation on method "a" yielding twinning defects, and (d–f) thermal decomposition of iron oleate. TEM and magnetic measurements (MAG) were used to determine polydispersities (%) and log-normal size distributions, scaled to the maximum probability P_{max}. Both the TEM and magnetic size distributions are shown as number density distributions. For better comparison with crystallite sizes from X-ray diffraction line broadening (XRD), volume-averaged TEM and MAG sizes are indicated by large circular dots.

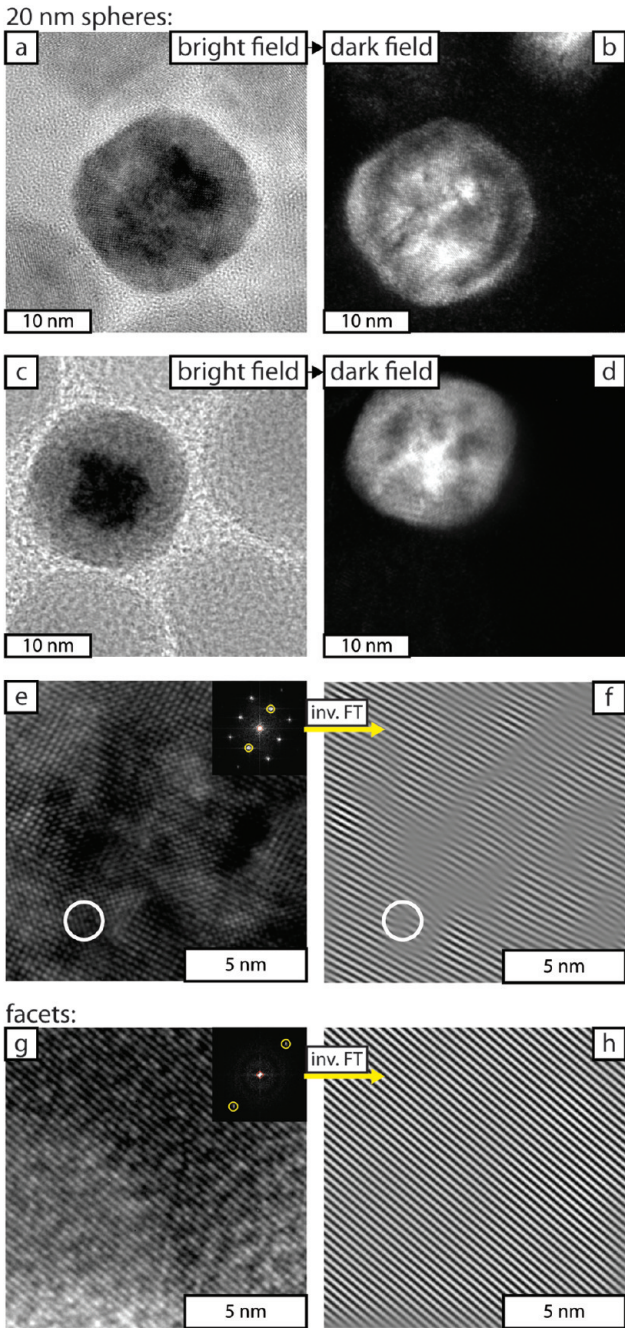

Figure 2. High-resolution TEM images of two 20 nm "sphere" particles (a–f) and a 20 nm "facet" particle (g,h). Each 20 nm "sphere" exhibits defect-induced internal contrast variations, both in bright field mode (a,c) and in dark-field visualization of the diffracted electrons (b,d). At higher magnification, the effect of crystal lattice defects in e and g is visually enhanced by Fourier transform (insets), followed by inverse Fourier transform (inv.FT) of the indicated spots in Fourier space, pertaining to only one crystallographic direction. Several dislocations are then revealed in the "sphere" (see, for instance, inside the circle) but none in the "facet".

and magnetic measurements give a similar average size and polydispersity. However, for the "twins" and the "spheres" of 17 and 20 nm, the magnetic sizes are much smaller and more polydisperse than the geometric sizes. Nevertheless, the saturation magnetization measured on dry particles was of the expected order of magnitude (see Table 1). The measurements from which the magnetic distributions in Figure 1 were calculated will now be further discussed.

Figure 3 illustrates the effect of the size of the nanoparticle dipoles on the magnetization curve. Large dipoles result in a steep initial slope because a weak field suffices to align them, whereas small dipoles require a much stronger field to approach saturation magnetization. This implies that the field-dependence

dx.doi.org/10.1021/jp203373f |J. Phys. Chem. C 2011, 115, 14598–14605

Table 1. Summary of Numerical Results, Including Number-Averaged Sizes, $\langle d \rangle$; Volume-Averaged Sizes, $\langle d^3 \rangle^{1/3}$; and Size Polydispersities, σ_d

sample name		20 nm facets	precipitates	20 nm twins	8 nm spheres	17 nm spheres	20 nm spheres
ref to synthesis method		31−33	40, 41		43, 44	43, 44	43, 44
part of Figure *1*		a	b	c	d	e	f
internal crystal defects		∼none	∼none	twinning	∼none	dislocations	dislocations
TEM	$\langle d \rangle$ (nm)	20.0	8.0	19.7	8.4	16.6	19.6
	$\langle d^3 \rangle^{1/3}$ (nm)	20.4	8.9	20.1	8.5	16.6	20.0
	σ_d (%)	12	31	10.7	8.8	3.5	11.6
XRD	$\langle d^3 \rangle^{1/3}$ (nm)	18 [a]	9	13	8	13	13
AGM	$\langle d \rangle$ (nm)	15.8	6.7	5.7	6.3	4.7	5.2
	$\langle d^3 \rangle^{1/3}$ (nm)	16.3	7.7	6.7	6.5	5.3	6.3
	σ_d (%)	17	38	40	14	35	41
	$\langle m \rangle$ (10^{-20} Am^2)	107.0	11.1	7.5	6.7	3.7	6.1
	M_{sat} of dry particles, including oleic acid (emu/g)	69 [a]	53	65	26	28	30

[a] Measured on a separate batch of particles prepared by the same method ($\langle d \rangle$ = 23.5 nm).

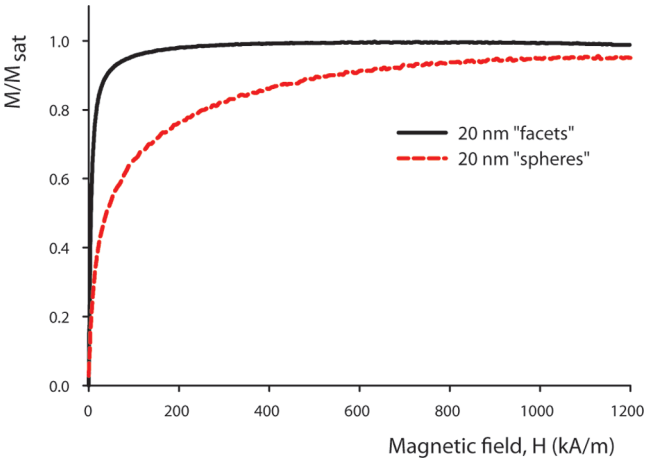

Figure 3. Illustration of how the average magnetic dipole moment affects the magnetization curve of ferrofluids. Magnetization curves are shown for iron oxide "facet" and "sphere" particles with a similar geometric size of 20 nm, dispersed in the apolar solvent decalin. The magnetizations are scaled to the saturation value. Clearly, the dipole moment of the "facet" particles is much larger than that of the "spheres", since the "facets" require a much weaker magnetic field to align the dipoles.

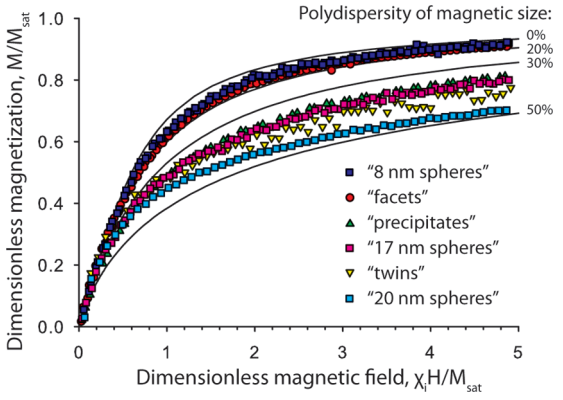

Figure 4. Dimensionless magnetization curves of the iron oxide nanoparticles imaged in Figure 1, measured on dilute dispersions to avoid the effects of nanoparticle dipole interactions. The magnetization, M, is scaled to its saturation value, M_{sat}, and the magnetic field, H, is scaled using M_{sat} and the initial magnetic susceptibility, χ_i, to yield an initial slope of unity. In this way, the curves do not depend on the average value but only on the polydispersity and distribution shape of the magnetic dipole moment. The drawn lines are simulated curves for log-normal distributions of the magnetic size with a standard deviation of 0, 20, 30, and 50%. Only a low-field selection of the data is presented here.

of the *relative* magnetization is sufficient information to determine the magnitude of the magnetic dipole moment of nanoparticles. No knowledge of the mass of the sample is required. However, it is necessary to know the magnetization at which the sample saturates (M_{sat}), which was determined by numerically fitting the entire curve. The M_{sat} value was verified by extrapolating the magnetization M versus reciprocal field, $1/H$, to obtain the magnetization in the limit that $1/H$ approaches zero.

The polydispersity of the magnetic dipole moment is obtained from the *shape* of the magnetization curve. To demonstrate this, we represent a low-field selection of the magnetization data using two dimensionless axes in Figure 4. Not only is the magnetization (corrected for diamagnetic contributions) scaled to its saturation value, as in Figure 3, but now also the magnetic field strength is rescaled in such a way that the initial slope is unity. This rescaling is performed using the measured initial magnetic susceptibility, that is, the slope χ_i of M versus H in the low-field limit. For a given magnetic polydispersity, σ_m, pertaining to a specific distribution shape (for instance, log-normal), any chosen value of the dimensionless field corresponds to a unique value of the dimensionless magnetization, independent of the magnitude of the dipole moments; the reason is that from eqs 2 and 3, an increase of m^* by a factor of x increases M by a factor $\exp[(\ln x)^2/2\sigma_m^2]$, and it can be shown that M_{sat} and χ_i are then increased by the same factor. For monodisperse dipole moments, the curve shape is given by the Langevin function, whereas for magnetically polydisperse ferrofluids, the dimensionless magnetization at a chosen value of the dimensionless magnetic field is lower because the small dipoles of the distribution lag behind in being aligned. To the best of our knowledge, our dimensionless representation of the magnetization data is original and a convenient way to compare the magnetic polydispersity in experimental systems without having to assume a log-normal or other type of distribution.

3.3. X-ray Diffraction. For all the particles studied, the positions of the XRD diffraction peaks indicate the presence of

magnetic iron oxide, magnetite (Fe_3O_4) or maghemite (γ-Fe_2O_3) or both, which is difficult to distinguish from XRD (see the Supporting Information). For the spheres, this concurs with Park et al.,[43] who reported that crystal composition gradually shifts from maghemite to magnetite for increasing particle sizes. The two crystal forms have a similar theoretical bulk magnetization.[52] The average nanoparticle sizes obtained from XRD line broadening are shown in Figure 1 as vertical lines. There was insufficient material of the "facet" particles to perform XRD on the same synthesis batch of particles that were studied extensively in the past by various techniques,[34−39,45] but a new synthesis batch of such particles yielded particles with a TEM size of 23 nm and an XRD size of 18 nm. XRD provides a volume-weighted average. Therefore, for better comparison with XRD, the volume-averaged sizes from TEM and magnetic measurements are indicated by a large circular dot on each TEM and magnetization curve analysis (MAG) distribution curve in Figure 1.

The numerical results from TEM, AGM, and XRD are summarized in Table 1.

4. DISCUSSION

Magnetic iron oxide nanoparticles were prepared with different degrees of crystallinity, and the effective sizes were determined by electron microscopy, magnetization curve analysis, and X-ray diffraction. Here, first the sizes measured by different methods are compared with each other to conclude which types of particles are single crystals and single magnetic domains. This information is then used to examine how twinning defects and dislocations affect the nanoparticle magnetic dipole moment and, in particular, its polydispersity. Finally, it is discussed how the magnetic properties are related to the chemical synthesis method.

An XRD size that agrees with the volume-averaged TEM size indicates that each nanoparticle is a single crystal. This is the case for the "facets", the "precipitates", and the 8 nm "spheres" (Figure 1 and Table 1). In contrast, the XRD size of the "twins" and the largest "spheres" is significantly smaller than expected from TEM. In the case of the twinned particles, this is clearly due to the twinning defects, which split each particle into two or more crystalline domains. For the 17 and 20 nm "spheres", XRD and high-resolution TEM (Figure 2) suggest that the high density of dislocations perturbs the long-range periodicity to such a large extent that these particles are also split into several crystalline domains.

The magnetic sizes as calculated by us on the basis of the theoretical bulk magnetization are expected to agree with TEM and XRD when the particles are single crystalline and sufficiently small that they have a single magnetic domain. This is, indeed, what is observed for the "facets", the "precipitates", and the 8 nm "spheres". In these cases, the magnetic size is only slightly smaller than from TEM and XRD. This small difference is ascribed to surface defects.[14,27−30]

For the twinned particles and the largest "spheres", however, the volume-averaged effective magnetic size (the large circular dots in Figure 1) is less than half that from XRD. Nevertheless, the saturation magnetization M_{sat} of the dry particles is of the expected order of magnitude. The small magnetic size appears to be that of individual magnetic domains inside each particle, which respond separately to the external field. The magnetocrystalline anisotropy of magnetic iron oxides is sufficiently low and the magnetic domains are apparently sufficiently small that rapid Néel reorientation of the dipoles inside separate magnetic domains seems plausible.[16] The dislocations and possibly also an inhomogeneous magnetite/maghemite stoichiometry disrupt the long-range coupling of atomic magnetic spins. This agrees with the detrimental effects of crystal defects on the magnetic properties of bulk crystalline magnetite.[59] In our case with nanoparticles, a consequence of the fact that the crystalline defects are not well controlled is that the magnetic properties can be very different from one particle to another. In other words, the magnetic polydispersity is much higher than expected from the geometric size polydispersity.

To promote uniform magnetic properties, not only must the geometric size polydispersity be low but also internal crystal defects must be avoided. One approach to obtain a low concentration of crystal defects is to grow particles in separate seeded growth steps. In the optimal case, this results in epitaxial growth in each step, as was done for the "facet" particles. However, this approach is laborious, and in each growth step, a mishap may occur, resulting, for instance, in twinning defects that are propagated in subsequent growth steps. In that respect, single-step thermal decomposition of iron oleate, with a nanoparticle size tunable via the boiling point of the solvent, is much more convenient. Our "sphere" particles of 8 nm prepared in that way are well crystallized and have a magnetic size polydispersity on the same order as the geometric size polydispersity. However, when larger spherical particles of 17 or 20 nm were prepared by the same method, high concentrations of internal crystal defects were obtained, which decreased the net magnetic moment of the particles in low field and increased the magnetic polydispersity.

A possible remedy for crystal defects is to recrystallize the particles by annealing them, as was done by Kwon et al.[44] by refluxing for 15 h at 320 °C. In that process, the magnetic moment increased by a factor of 5, approaching the theoretical bulk magnetization; at the same time, the shape of the particles changed from sphere to cube, and the geometric size polydispersity increased. One might be tempted to conclude that the shape change from sphere to cube is directly responsible for the increased dipole moment, but this is not necessarily the case. Salazar-Alvarez et al.[60] compared the magnetic properties of spherical and cubic iron oxide nanoparticles of the same volume, and they found practically the same magnetic properties, the main difference being only the blocking temperature. In light of our own results, the increased magnetic moment after the annealing of spherical iron oxide nanoparticles by Kwon et al.[44] was probably mainly due to the removal of internal crystal defects.

A possible conclusion is that better magnetic properties are to be expected from iron oxide nanoparticles whose surface is faceted rather than spherical. Facets suggest that particle growth was sufficiently slow for the preferential development of energetically favored surface crystal planes. In contrast, sphericity suggests that particle growth is too rapid to develop those facets, which may also be too rapid for good crystallization by epitaxial growth. Our own spherical particles were prepared in a single step, implying relatively rapid nucleation and growth. Good crystallinity and magnetic properties are found for the particles of 8 nm but not for the larger spherical particles of 17 or 20 nm. Their growth was probably even more rapid, resulting in a high concentration of crystal defects and poor magnetic properties. Despite their low geometric size polydispersity, the 17 and 20 nm "spheres" have a high magnetic polydispersity on the same order as when particles are prepared by aqueous precipitation.

5. CONCLUSIONS

In conclusion, low TEM size polydispersity of magnetic nanoparticles does not guarantee low polydispersity of the magnetic dipole moments. During chemical synthesis, effective separation of nucleation and growth results in a low geometric size polydispersity. Assuming that each particle has a single magnetic domain, is perfectly crystallized, and has the same shape, low geometric size polydispersity would result in low polydispersity of the magnetic properties. However, it is difficult to avoid crystal defects, such as twinning and dislocations, which can have a highly detrimental effect on the strength and low polydispersity of the magnetic properties. For applications in which the magnetic properties of the individual particles are critical, TEM size monodispersity therefore does not suffice as a criterion for a successful synthesis. The magnetic properties may be much more polydisperse than expected from the physical size.

■ ASSOCIATED CONTENT

Supporting Information. Characterization results for the discussed iron oxide nanoparticles, including magnetization curves, TEM images, X-ray diffraction patterns. This material is available free of charge via the Internet at http://pubs.acs.org.

■ AUTHOR INFORMATION

Corresponding Author
*E-mail: b.h.erne@uu.nl.

■ ACKNOWLEDGMENT

We thank John Geus, Jan Hilhorst, Andrei Petukhov, Mark Klokkenburg, Jos van Rijssel, Aldo Brinkman, Janne-Mieke Meijer, and Pedro Zeijlmans van Emmichoven for helpful discussions. This work was supported by The Netherlands Organisation for Scientific Research (NWO).

■ REFERENCES

(1) Sun, S. H.; Murray, C. B.; Weller, D.; Folks, L.; Moser, A. *Science* **2000**, *287*, 1989.
(2) Zeng, H.; Li, J.; Liu, J. P.; Wang, Z, L.; Sun., S. H. *Nature* **2002**, *420*, 395.
(3) Pankhurst, Q. A.; Connolly, J.; Jones, S. K.; Dobson, J. *J. Phys. D: Appl. Phys.* **2003**, *36*, R167.
(4) Gupta, A. K.; Gupta, M. *Biomaterials* **2005**, *26*, 3995.
(5) Jeong, U.; Teng, X. W.; Wang, Y.; Yang, H.; Xia, Y. N. *Adv. Mater.* **2007**, *19*, 33.
(6) Lu, A. H.; Salabas, E. L.; Schuth, F. *Angew. Chem., Int. Ed.* **2007**, *46*, 1222.
(7) Laurent, S.; Forge, D.; Port, M.; Roch, A.; Robic, C.; Elst, L. V.; Muller, R. N. *Chem. Rev.* **2008**, *108*, 2064.
(8) Gao, J. H.; Gu, H. W.; Xu, B. *Acc. Chem. Res.* **2009**, *42*, 1097.
(9) Pankhurst, Q. A.; Thanh, N. K. T.; Jones, S. K.; Dobson, J. *J. Phys. D: Appl. Phys.* **2009**, *42*, 224001.
(10) Talapin, D. V.; Lee, J. S.; Kovalenko, M. V.; Shevchenko, E. V. *Chem. Rev.* **2010**, *110*, 389.
(11) Shylesh, S.; Schunemann, V.; Thiel, W. R. *Angew. Chem., Int. Ed.* **2010**, *49*, 3428.
(12) Hao, R.; Xing, R. J.; Xu, Z. C.; Hou, Y. L.; Gao, S.; Sun, S. H. *Adv. Mater.* **2010**, *22*, 2729.
(13) Krishnan, K. M. *IEEE Trans. Magn.* **2010**, *46*, 2523.
(14) Batlle, X.; Labarta, A. *J. Phys. D: Appl. Phys.* **2002**, *35*, R15.
(15) Gonzales-Weimuller, M.; Zeisberger, M.; Krishnan, K. M. *J. Magn. Magn. Mater.* **2009**, *321*, 1947.
(16) Rosensweig, R. E. *J. Magn. Magn. Mater.* **2002**, *252*, 370.
(17) Khandhar, A. P.; Ferguson, R. M.; Krishnan, K. M. *J. Appl. Phys.* **2011**, *109*, 07B310.
(18) Fannin, P. C. *J. Magn. Magn. Mater.* **1994**, *136*, 49.
(19) Ferguson, R. M.; Minar, K. R.; Khandhar, A. P.; Krishnan, K. M. *Med. Phys.* **2011**, *38*, 1619.
(20) Gleich, B.; Weizenecker, J. *Nature* **2005**, *435*, 1214.
(21) Sattel, T. F.; Knopp, T.; Biederer, S.; Gleich, B.; Weizenecker, J.; Borgert, J.; Buzug, T. M. *J. Phys. D: Appl. Phys.* **2009**, *42*, 022001.
(22) Murray, C. B.; Kagan, C. R.; Bawendi, M. G. *Annu. Rev. Mater. Sci.* **2000**, 545.
(23) Park, J.; Joo, J.; Kwon, S. G.; Jang, Y.; Hyeon, T. *Angew. Chem., Int. Ed.* **2007**, *46*, 4630.
(24) Kwon, S. G.; Hyeon, T. *Acc. Chem. Res.* **2008**, *41*, 1696.
(25) Hergt, R.; Dutz, S.; Müller, R.; Zeisberger, M. *J. Phys.: Condens. Matter* **2006**, *18*, S2919.
(26) Andrés Vergés, M.; Costo, R.; Roca, A. G.; Marco, J. F.; Goya, G. F.; Serna, C. J.; Morales, M. P. *J. Phys. D: Appl. Phys.* **2008**, *41*, 134003.
(27) Kodama, R. H. *J. Magn. Magn. Mater.* **1999**, *200*, 359.
(28) Barker, A. J.; Cage, B.; Russek, S.; Stoldt, C. R. *J. Appl. Phys.* **2005**, *98*, 063528.
(29) Goya, G. F.; Berquó, T. S.; Fonseca, F. C.; Morales, M. P. *J. Appl. Phys.* **2003**, *94*, 3520.
(30) Roca, A. G.; Morales, M. P.; O'Grady, K.; Serna, C. J. *Nanotechnology* **2006**, *17*, 2783.
(31) Klokkenburg, M.; Vonk, C.; Claesson, M.; Meeldijk, J.; Erné, B.; Philipse, A. *J. Am. Chem. Soc.* **2004**, *126*, 16706.
(32) Sun, S.; Zeng, H. *J. Am. Chem. Soc.* **2002**, *124*, 8204.
(33) Sun, S.; Zeng, H.; Robinson, D. B.; Raoux, S.; Rice, P. M.; Wang, S. X.; Li, G. *J. Am. Chem. Soc.* **2004**, *126*, 273.
(34) Klokkenburg, M.; Dullens, R. P. A.; Kegel, W. K.; Erné, B. H.; Philipse, A. P. *Phys. Rev. Lett.* **2006**, *96*, 037203.
(35) Klokkenburg, M.; Erné, B. H.; Meeldijk, J. D.; Wiedenmann, A.; Petukhov, A. V.; Dullens, R. P. A.; Philipse, A. P. *Phys. Rev. Lett.* **2006**, *97*, 185702.
(36) Klokkenburg, M.; Erne, B. H.; Wiedenmann, A.; Petukhov, A. V.; Philipse, A. P. *Phys. Rev. E* **2007**, *75*, 051408.
(37) Wiedenmann, A.; Keiderling, U.; Meissner, M.; Wallacher, D.; Gaehler, R.; May, R. P.; Prevost, S.; Klokkenburg, M.; Erne, B. H.; Kohlbrecher, J. *Phys. Rev. B* **2008**, *77*, 184417.
(38) Georgescu, M.; Klokkenburg, M.; Erne, B. H.; Liljeroth, P.; Vanmaekelbergh, D.; van Emmichoven, P. A. Z. *Phys. Rev. B* **2006**, *73*, 184415.
(39) Klokkenburg, M.; Erne, B. H. *J. Magn. Magn. Mater.* **2006**, *306*, 85.
(40) Bica, D. *Rom. Rep. Phys.* **1995**, *47*, 265.
(41) Massart, R. *IEEE Trans. Magn.* **1981**, *17*, 1247.
(42) Erné, B. H.; van den Pol, E.; Vroege, G. J.; Wensink, H. H. *Langmuir* **2005**, *21*, 1802.
(43) Park, J.; An, K.; Hwang, Y.; Park, J.-G.; Noh, H.-J.; Kim, J.-Y.; Park, J.-H.; Hwang, N.-M.; Hyeon, T. *Nat. Mater.* **2004**, *3*, 891.
(44) Kwon, S. G.; Piao, Y.; Park, J.; Angappane, S.; Jo, Y.; Hwang, N.-M.; Park, J.-G.; Hyeon, T. *J. Am. Chem. Soc.* **2007**, *129*, 12571.
(45) Klokkenburg, M.; Erné, B. H.; Mendelev, V.; Ivanov, A. O. *J. Phys.: Condens. Matter* **2008**, *20*, 204113.
(46) Krawitz, A. D. *Introduction to Diffraction in Materials Science and Engineering*; John Wiley: New York, 2001; pp 146−166.
(47) Chantrell, R. W.; Popplewell, J.; Charles, S. W. *IEEE Trans. Magn.* **1978**, *14*, 975.
(48) Rasa, M. *Eur. Phys. J. E* **2000**, *2*, 265.
(49) Chen, D.-X.; Sanchez, A.; Taboada, E.; Roig, A.; Sun, N.; Gu, H.-C. *J. Appl. Phys.* **2009**, *105*, 083924.
(50) Taketomi, S.; Shull, R. D. *J. Appl. Phys.* **2002**, *91*, 8546.
(51) Ivanov, A. O.; Kuznetsova, O. B. *Colloid J.* **2006**, *68*, 430.
(52) Chikazumi, S. *Physics of Magnetism*; Wiley: New York, 1964.
(53) Williams, D. B.; Carter, C. B. *Transmission Electron Microscopy: a Textbook for Materials Science*; Plenum: New York, 1996.

(54) Hull, D.; Bacon, D. J. *Introduction to Dislocations*; Butterworth-Heinemann: Woburn, MA, 2001.
(55) Arakawa, K.; Ono, K.; Isshiki, M.; Mimura, K.; Uchikoshi, M.; Mori, H. *Science* **2007**, *318*, 956.
(56) Holm, C.; Weis, J.-J. *Curr. Opin. Colloid Interface Sci.* **2005**, *10*, 133–140.
(57) Huke, B.; Lücke, M. *Rep. Prog. Phys.* **2004**, *67*, 1731.
(58) Bae, C. J.; Angappane, S.; Park, J.-G.; Lee, Y.; Lee, J.; An, K.; Hyeon, T. *Appl. Phys. Lett.* **2007**, *91*, 102502.
(59) Ozdemir, O.; Dunlop, D. J. J. *Geophys. Res.* **1997**, *102*, 20211.
(60) Salazar-Alvarez, G.; Qin, J.; Šepelák, V.; Bergmann, I.; Vasilakaki, M.; Trohidou, K. N.; Ardisson, J. D.; Macedo, W. A. A.; Mikhaylova, M.; Muhammed, M.; Baró, M. D.; Nogués, J. *J. Am. Chem. Soc.* **2008**, *130*, 13234.